Available online at www.sciencedirect.com

ScienceDirect

Procedia Structural Integrity 17 (2019) 643–650

Structural Integrity Procedia

www.elsevier.com/locate/procedia

ICSI 2019 The 3rd International Conference on Structural Integrity

Fatigue damage analysis of offshore wind turbine monopile weldments

Romali Biswal*, Ali Mehmanparast

Renewable Energy Systems Centre, Cranfield University, UK

Abstract

Offshore wind turbines (OWT) are subjected to harsh environmental conditions in addition to the variable service loads. The present study is aimed at performing a realistic fatigue life estimation of the monopile structure using operational service loads recorded by online monitoring systems. Fatigue damage analysis has been conducted at the circumferential weld joints using finite element (FE) method by considering geometrical and material property discontinuities. Global-local modelling of the OWT was performed in as-welded condition to capture the local stress range at the weld toe, which acts as the critical site where cracks are most likely to initiate and propagate. The S-N fatigue design approach and maximum stress range at the weld toe have been used to determine the fatigue crack initiation life in monopiles. The results from the proposed approach show that a realistic life assessment can be made on monopile structures by accounting for the geometrical effects at the circumferential welds.

© 2019 The Authors. Published by Elsevier B.V.
Peer-review under responsibility of the ICSI 2019 organizers.

Keywords: Offshore structures; S355 steel; SCADA online monitoring; Finite element modelling; Fatigue life prediction.

1. Introduction

The resources for renewable energy sources are derived straight from the environment, hence enables power generation with little to no greenhouse gas emissions. The European Environment Agency report (EEA, 2019) shows that Europe and China have taken initiatives to advance the technology towards cleaner and greener energy, Fig. 1.

* Corresponding author. Tel.: +44-1234-758331 .
E-mail address: a.mehmanparast@cranfield.ac.uk

2452-3216 © 2019 The Authors. Published by Elsevier B.V.
Peer-review under responsibility of the ICSI 2019 organizers.
10.1016/j.prostr.2019.08.086

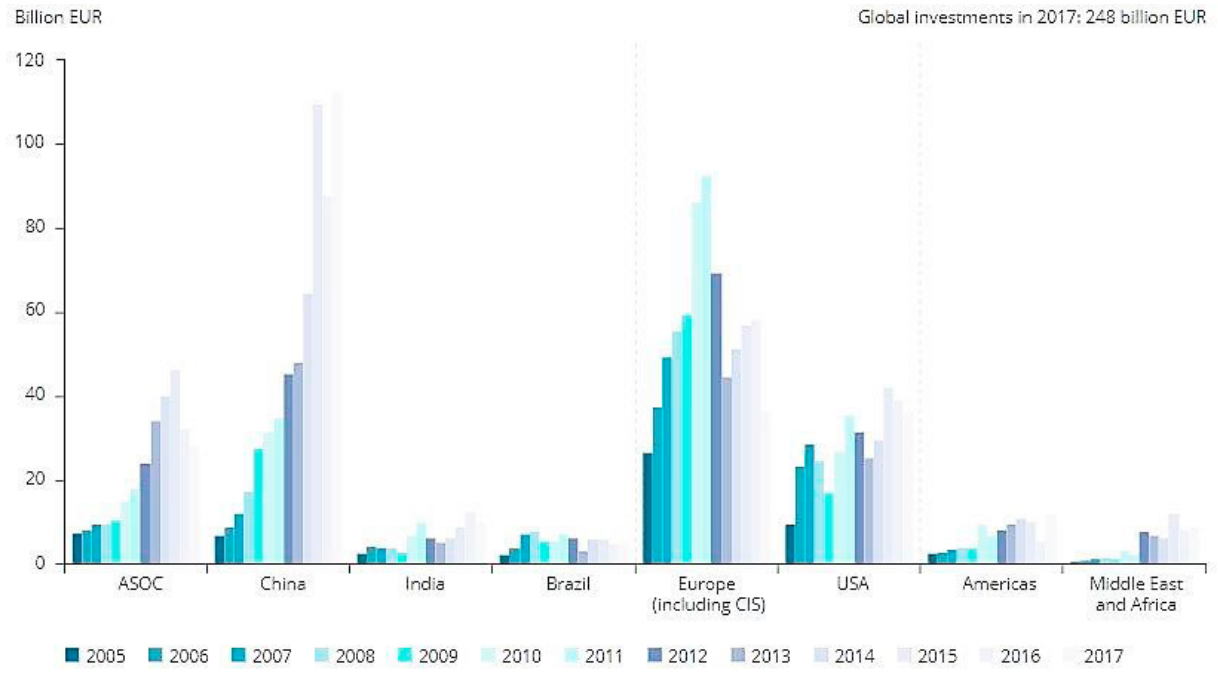

Fig. 1 Total new investments made towards adopting renewable energy between 2015 and 2017.

Over the last 30 years, power generation using wind energy has emerged as a sustainable technology. The installation of offshore wind turbines (OWT) across Europe has been growing rapidly, leading to the total installed wind energy capacity growing from 84 GW in 2010 (Zervos, 2011), 128 GW in 2014 (Giorgio, Ho and Pineda, 2015) and 189 GW in 2018 (Komusanac, Fraile and Brindley, 2018). Currently, wind energy meets 14% of the European electricity demands, thereby making it the second largest power generation capacity in Europe after gas installations (Igwemezie, Mehmanparast and Kolios, 2019). Further, the estimations given by the European Wind Energy Association (EWEA) predict that by the year 2030, the total installed capacity will supply 23% of the total energy demands in Europe (van Wingerde *et al.*, 2018).

From inspection and maintenance perspective, the foundation structures are known to have the highest complexity. Typical OWT foundation structures include monopile, jacket and floating structures. Currently, shallow water installations (< 40m depth) are widely used, which makes monopile structures as the preferred foundation type. The manufacturing of a monopile includes hot-rolled plates of 30-125mm thickness to be bent (via cold rolling) and longitudinally welded to form 'cans' of 3-7m diameter. The 'cans' are subsequently joined via circumferential welding to achieve the full length of the structure (Jacob *et al.*, 2018). At present, the design standards for these monopiles have been adopted from the offshore oil and gas industry, since it is the only sector with experience of offshore installations. However, the size scales of OWT structures are an order of magnitude or more greater, which eventually leads to overdesigning of the OWT and higher capital costs. Therefore, it is essential to monitor the service loads acting on offshore monopile structures and develop more informed design criteria for the wind energy sector.

This study aims to investigate the effect of the operational service loads on the monopile structure. Since welding introduces material and geometrical non-linearity, two of the most critical circumferential weldments were included in the analysis. The local stress range at the weld toe was calculated using elastic-plastic finite element analysis and used for predicting the fatigue crack initiation life of the monopile structure.

2. Material property

The material properties for EN-10225:09 S355 G10+M were taken from the literature (DNV GL, 2016; Jacob *et al.*, 2018), where a cross-welded specimen was tested to determine the tensile behaviour of the base metal, weld

metal and the heat affected zone by measuring the strain at the specific sections using digital image correlation technique. Fig. 2(a) shows the stress vs. plastic strain response (Jacob *et al.*, 2018), which was used in this study to conduct an elastic-plastic FE analysis.

Further, the intrinsic material property constants for the basic fatigue design curve, Eq. (1), were taken from the DNVGL-RP-C203 standard for offshore steel structures (DNV GL, 2016). Fig. 2(b) shows the fatigue life of tubular joints tested in various environmental conditions. In this study, the seawater free corrosion curve was used to follow a conservative approach for fatigue damage estimation.

$$\log N = \log \bar{a} - m \log \Delta\sigma \tag{1}$$

where N is the number cycles to failure for an applied stress range of $\Delta\sigma$, m and $\log \bar{a}$ are the negative inverse slope and the intercept of S-N curve, respectively. The values of m and $\log \bar{a}$ are 3 and 12.03 for seawater free corrosion (DNV GL, 2016).

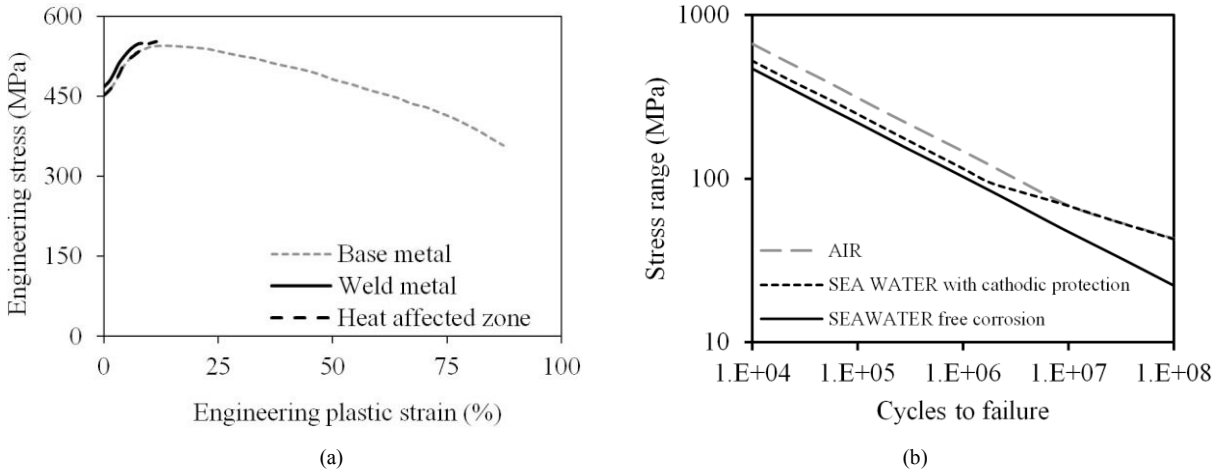

Fig. 2 (a) Tensile behaviour of different sections of cross-welded S355 specimen reported in literature (Jacob *et al.*, 2018), (b) S-N curves for tubular joints in air and sea water environment recommended by DNVGL-RP-C203 standard.

3. Finite element modelling

3.1. Material model

The constitutive relationship for the material was modelled using a linear kinematic hardening/softening algorithm available in Abaqus library. The uniaxial test data presented in Fig. 2(a) was input in tabular format to calibrate the stress-strain relationship. The von Mises yield criterion was selected to determine the onset of plastic deformation.

3.2. Monopile Structure

The monopile was modelled using a 3-D cylindrical geometry in the commercial ABAQUS® software. The monopile, transition piece, tower and hub was modelled as a single cylindrical structure. The total length of the monopile was assumed to be 65m, of which only 20m lies above the mud line as shown in Fig. 3(a). Two circumferential weldments nearest to the mudline were modelled. It was assumed that the height to diameter ratio of the ‘cans’ constituting the monopile structure was 1. Therefore, the separation between the circumferential welds was 6.5m, resulting in the first circumferential weld above the mud line to be located 4m from the mud line and the next weld was placed 6.5m apart from the first weld. The dimensions of the crown height, crown width, weld toe radius and the size of heat affected zone (HAZ) were taken from the published literature as shown in Fig. 3(b)

(Jacob *et al.*, 2018). The true shape of the HAZ through the thickness was reported to be triangular, however, in this study the shape was assumed to be rectangular as shown in the schematic of the weld geometry in Fig. 3(c). Further, the weld geometry on the inner and outer wall was assumed to be identical.

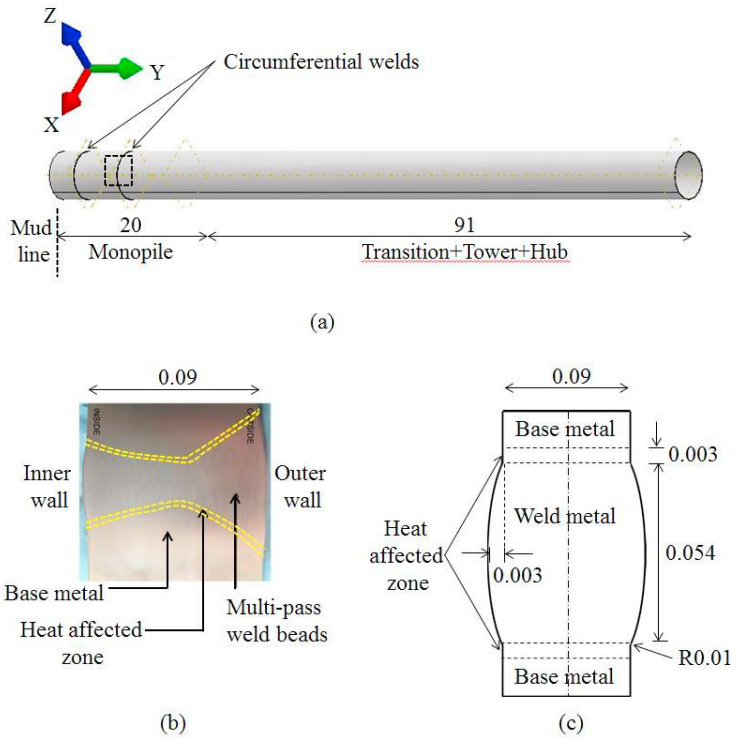

Fig. 3 (a) OWT model with sections above mud-line, (b) cross-sectional view of circumferential weld geometry (Jacob et al., 2018), (c) schematic of region highlighted in (a) showing the idealised weld geometry used in the FE model. [Note: all dimensions are in meter].

3.3. Service loads and boundary conditions

Through online monitoring systems such as supervisory control and data acquisition (SCADA) system and WAVEbuoy, the service loads acting on an OWT was collected from an offshore wind farm. The wind data was recorded every 10 mins and the wave data every 30 mins. The wind profile measurements included wind speed and direction, rotational velocity of shaft, relative positioning of blades and power generation; while the wave profile measurements included the wave height and time period. Further the ambient temperature, pressure and humidity variation was also documented. The wind loads acting on the OWT were calculated using the blade element momentum theory (van Wingerde *et al.*, 2018) and Morison's semi-empirical approach (Lombardi, Bhattacharya and Nikitas, 2017) was used to calculate the wave loads on the submerged structure. The calculated wind and wave loads were then grouped into six load cases using rain flow counting implemented using MATLAB®. It was assumed that the wind and wave loads are proportional; therefore, the wind and wave load inputs in ABAQUS was limited to six load levels, where the least wind load corresponds to the smallest wave load and vice versa. Table 1 shows the load cases modelled in the FE analysis. Fixed boundary condition was applied to the embedded section of the monopile.

Table 1. Loads applied to the FE model.

Load case	Probability of load case	Wind load (kN)			Wave load (kN)		
		Blade	Tower	Frequency (Hz)	Inertia	Drag	Frequency (Hz)

1	0.6119	217	2	0.0035	190	1	0.225
2	0.2986	515	12	0.0075	462	6	0.2
3	0.0733	826	32	0.0125	773	17	0.175
4	0.0145	1145	61	0.0175	1067	38	0.15
5	0.0017	1466	100	0.0225	1343	72	0.13
6	0.0001	1769	145	0.0275	1483	105	0.12

3.4. Global-local modelling and fatigue damage calculation

The finite element size in the global model was varied between 0.5-0.1m, leading to 10340 elements as shown in Fig. 4(a). In order to capture the effect of stress concentration factor at the weld toe, the stress distribution from the overall model was applied as boundary condition to the sub-model consisting of the weldment nearest to the mud line as shown in Fig. 4(b) and (c). The finite element size in the sub-model was reduced to 0.02m, thereby resulting in 61500 elements in the sub-model. Linear brick element of 8 nodes (C3D8) was selected for the structure.

For every load case, the corresponding maximum stress range was calculated by the sub-model and later applied to the S-N curve for sea water free corrosion recommended by DNVGL-RP-C203 standard to predict the fatigue crack initiation life according to notch-fatigue approach. Further, the expected number of fatigue cycles for each load case was estimated from probability given by the online monitoring data. It was assumed that linear cumulative damage was experienced by the OWT structure and the damage was calculated using Palmgren-Miner rule as shown in Eq. (2).

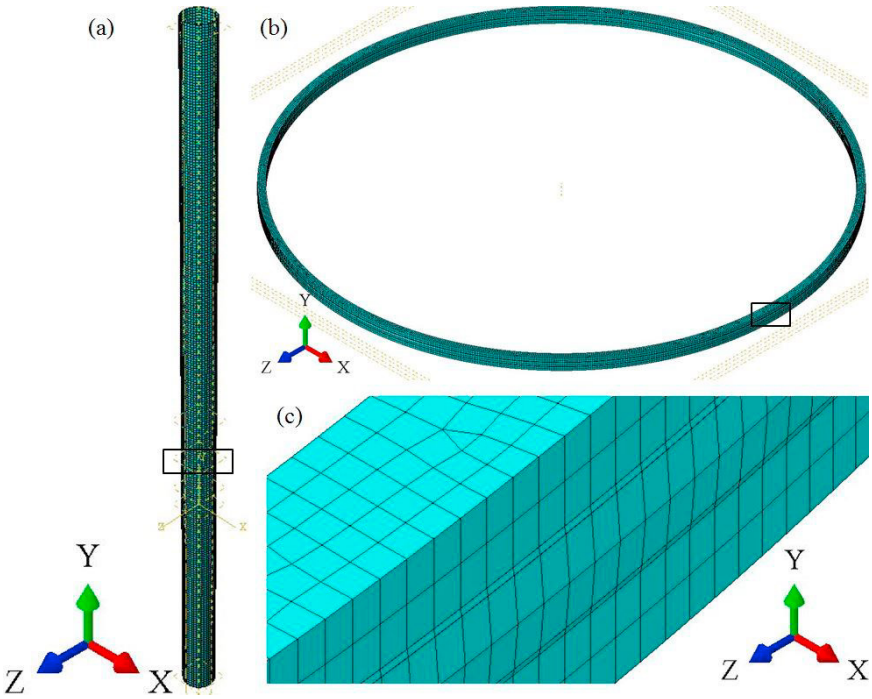

Fig. 4 Finite elements used in the study, (a) overall global mesh, (b) local mesh elements used in the sub-model, (c) enlarged view of the highlighted section from (b) to show the mesh elements.

$$D = \sum_{i=1}^{N_{lc}} \frac{n_i}{N_i} \tag{2}$$

where D is the damage in the monopile structure, N_{lc} the number of load cases considered, which in this study is six. For a particular nominal stress amplitude case i, n_i is the number of cycles acting on the monopile as counted by the rainflow algorithm and N_i the number of cycles leading to fatigue crack initiation, calculated by the S-N curve.

4. Results and discussions

4.1. Fatigue damage accumulation

Detailed analysis of the hot spot region was performed using sub-modelling approach. It was found that the weld toe acts as the highest stress region, Fig. 5. The maximum stress for each constant stress range block was computed as shown in Fig. 6(a). The stress range applicable for each load case is shown in Fig. 6(b) and was used in Eq. (1) to determine the corresponding cycles to failure. The fatigue damage calculation was then performed using Palmgren-Miner rule given in Eq. (2). For the highest operational stress level, i.e load case 6, the maximum stress range at the weld toe was 111 MPa. However, owing to the lowest probability corresponding to the highest load case, the damage caused to the OWT structure by this stress block was limited to 0.0002. The fatigue damage for the individual constant stress blocks are presented in Table 2. The total damage endured by the structure in 20 years of operation was found to be 0.03.

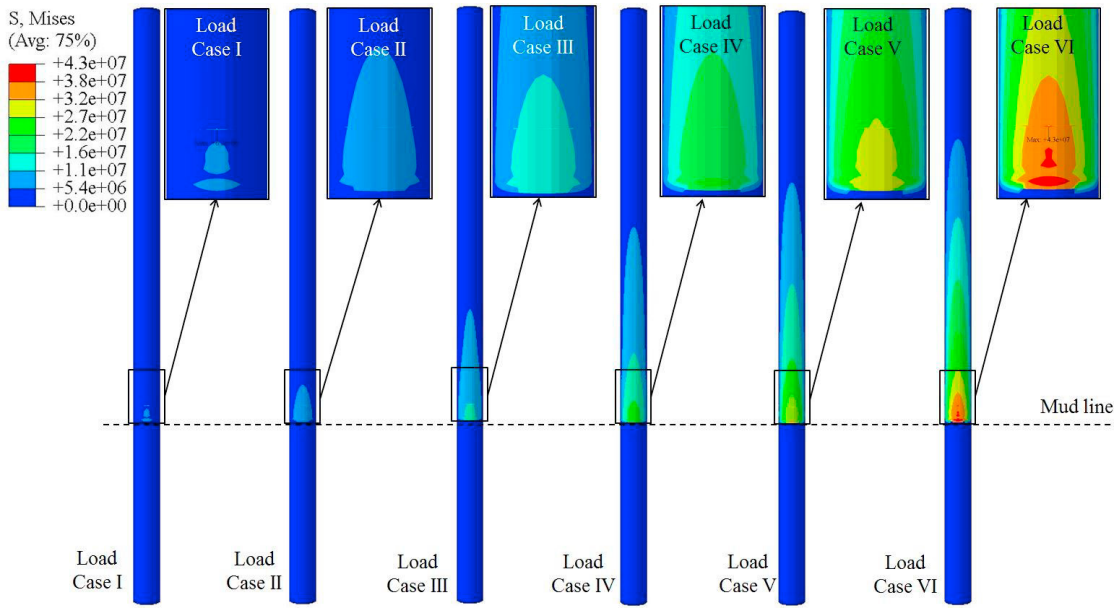

Fig. 5 Stress distribution profile at hotspot for the six constant stress range blocks. For each overall OWT view, an enlarged view of the hotspot is shown in upper right section.

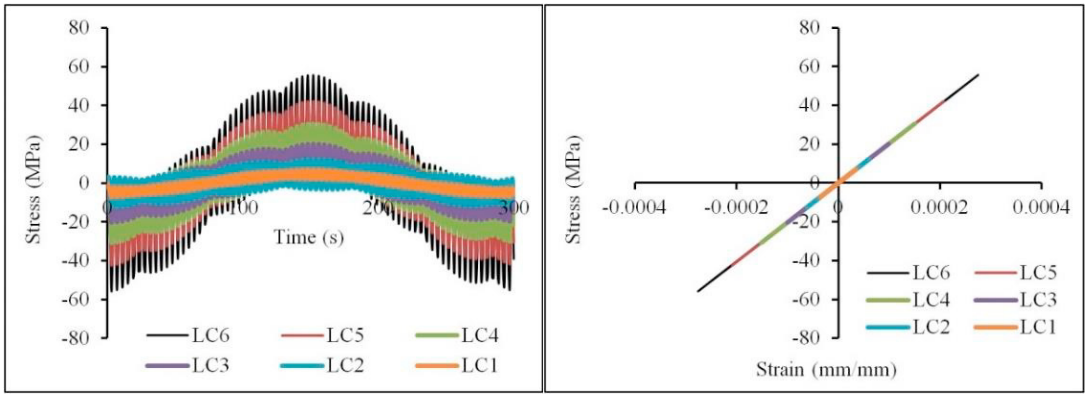

(a) (b)

Fig. 6 (a) Maximum stress vs. time acting on the weld toe in axial direction (y-axis), (b) stress range acting on the monopile weldment for each constant stress range block. [Legend LC stands for 'load case'. Refer Table 2 for values].

Table 2 Fatigue damage estimation for each constant stress block

Load case	Stress range (MPa)	No of cycles in 20 years (n_i)	Cycles to failure (N_i)	Damage (D)
1	14	1286459	3.73E+08	0.003452
2	25	627777	71066882	0.008834
3	40	154106	16325883	0.009439
4	61	30485	4678391	0.006516
5	84	3574	1792225	0.001994
6	111	210	775351	0.000271

5. Conclusions

Fatigue life estimation of the offshore wind turbine (OWT) was performed in this study using realistic weld geometry and loading conditions. The environmental factors such as wind speed, wave height etc. were monitored over a period of 2 years. The measured data was converted into representative service loads using semi-empirical methods. Finally, the stress and strain distribution at the most critical weld toe was evaluated by FE analysis. The findings are summarized below.

- Local stress profile at the weld toe was found to be well within the permissible limits for the structure.
- Total fatigue damage in 20 years of OWT operation was found to be 0.03 for the representative service loading conditions, therefore indicating that the OWT structural design is highly conservative.

In order to improve the prediction accuracy, the effect of residual stress and soil-pile interactions should be considered in the future work.

References

DNV GL (2016) 'Dnvgl-Rp-C203', (DNVGL-RP-C203), p. 176.

EEA (2019) *Renewable energy in Europe – 2018: Recent growth and knock-on effects*. doi: 10.2800/03040.

Giorgio, C., Ho, A. and Pineda, I. (2015) 'Wind energy scenarios for 2030', *Ewea*, (July), pp. 1–8. doi: 10.1017/CBO9781107415324.004.

Igwemezie, V., Mehmanparast, A. and Kolios, A. (2019) 'Current trend in offshore wind energy sector and material requirements for fatigue resistance improvement in large wind turbine support structures – A review', *Renewable and Sustainable Energy Reviews*. Elsevier Ltd, 101(November 2018), pp. 181–196. doi: 10.1016/j.rser.2018.11.002.

Jacob, A. *et al.* (2018) 'Residual stress measurements in offshore wind monopile weldments using neutron diffraction technique and contour method', *Theoretical and Applied Fracture Mechanics*. doi: 10.1016/j.tafmec.2018.06.001.

Komusanac, I., Fraile, D. and Brindley, G. (2018) 'Wind energy in Europe in 2018 - Trends and statistics'. Available at: https://windeurope.org/wp-content/uploads/files/about-wind/statistics/WindEurope-Annual-Statistics-2018.pdf.

Lombardi, D., Bhattacharya, S. and Nikitas, G. (2017) 'Physical Modeling of Offshore Wind Turbine Model for Prediction of Prototype Response', *Wind Energy Engineering: A Handbook for Onshore and Offshore Wind Turbines*, (1), pp. 353–374. doi: 10.1016/B978-0-12-809451-8.00017-5.

van Wingerde, A. M. *et al.* (2018) *Survey of support structures for offshore wind turbines*, *Tubular Structures XI*. doi:10.1201/9780203734964-7.

Zervos, A. (2011) 'Pure Power, A report by the European Wind Energy Association'.

https://dspace.org/

Fatigue damage analysis of offshore wind turbine monopile weldments

Biswal, Romali; Mehmanparast, Ali

2019-08-25
Elsevier
https://doi.org/10.1016/j.prostr.2019.08.086
Biswal R, Mehmanparast A. (2019) Fatigue damage analysis of offshore wind turbine monopile weldments. Procedia Structural Integrity, Volume 17, 2019, pp. 643-650

Downloaded from a DSpace repository. https://dspace.org/